48th AIAA Aerospace Sciences Meeting Including the New Horizons Forum and Aerospace Exposition
4 - 7 January 2010, Orlando, Florida

AIAA 2010-1566

Expansion tube investigation of shock stand-off distances in high-enthalpy CO_2 flow over blunt bodies

M. Sharma*, A.B. Swantek†, W. Flaherty‡, J. M. Austin§ and N. G. Glumac¶
University of Illinois at Urbana-Champaign, IL 61801

The shock standoff distance in front of a blunt body is sensitive to the thermochemical state of the free stream. Recently, experimental and numerical studies have reported significantly different bow shock profiles in high-enthalpy carbon dioxide flows, a discrepancy that may result from non-equilibrium processes during flow acceleration in ground-based facilities. In this work, an expansion tube is used to create a Mach 5.7 carbon dioxide flow, matching the stagnation enthalpy and the velocity of previous studies. Images of shock layers are obtained for spherical geometries and a scaled model of the Mars Science Lander. Different sphere diameters are used in order to access non-equilibrium and equilibrium stagnation line shock profiles predicted by theory. Mars Science Lander profiles at zero angle of attack are in good agreement with available data from the LENS X expansion tunnel facility, confirming results are facility-independent for the same type of flow acceleration, and indicating the flow velocity is a suitable first-order matching parameter for comparative testing. Heat transfer measurements on the Mars Science Lander are also presented for the three different angle of attacks, and the results are consistent with previous studies. Initial results from a proposed organo-metallic based emission spectroscopy technique for bow shock layer interrogation are also presented.

I. Introduction

In high-enthalpy hypersonic flight, thermochemical relaxation times are typically comparable to flow residence times, leading to nonlinear coupling between chemical reaction, vibrational excitation, and fluid mechanics. In carbon dioxide flows which are relevant to Martian planetary entry, thermochemical effects are particularly significant and may potentially be responsible for some recent anomalous results in blunt body shock layers. The hypersonic facilities at Calspan-University of Buffalo Research Center (CUBRC) have been central to the investigation of planetary entry flight conditions for many programs, including the up-coming Mars Science Laboratory (MSL) mission targeting exploration of the Martian surface. Recent studies revealed that the experimentally observed shock shape and stand-off distance differed significantly from numerical simulations

*Graduate Student, Department of Aerospace Engineering, University of Illinois, Member AIAA
†Graduate Student, Department of Aerospace Engineering, University of Illinois, Member AIAA
‡Graduate Student, Department of Aerospace Engineering, University of Illinois, Member AIAA
§Assistant Professor, Department of Aerospace Engineering, University of Illinois, Senior Member AIAA
¶Professor, Department of Mechanical Science and Engineering, University of Illinois, Member AIAA

over a 24" diameter MSL model for high-enthalpy test conditions at 5 and 10 MJ/kg in the LENS I reflected shock tunnel facility.[1] The computed shock stand-off distance for the 5 MJ/kg test condition was a factor of 2.25 times smaller than the experimental value. However, at a 2 MJ/kg test condition in the same facility, no such differences were observed. To examine this discrepancy further, the same model was tested in the LENS X expansion tube facility at 5 MJ/kg.[1] Excellent agreement was obtained between simulations and experiments in the LENS X facility.

It is possible that the discrepancy in the shock profiles observed in the different facilities at high enthalpies is due to the gas thermochemistry during the flow acceleration. In an expansion tube, the flow is accelerated to hypersonic velocities by an unsteady expansion wave which follows the primary shock. In a reflected shock tunnel, the flow is instead stagnated before being expanded through a nozzle, and chemical and thermal freezing which are commonly reported to occur downstream of the nozzle throat have been shown to alter the flowfield.[2–4]

It was proposed that the strong test gas expansion in the LENS I reflected-shock tunnel facility results in more complicated CO_2 relaxation processes than anticipated, which could account for increased levels of vibrational energy storage.[5] The numerical study found shock shape, stand-off distance, surface heat flux and pressure matched experiments when 42% of the total reservoir enthalpy was artifically frozen in vibrational energy.[5] As discussed by the authors, such high levels of vibrational freezing are not physical. The original simulations, for which the discrepancy with experiment exists, showed the vibrational energy to have relaxed to 3.6% of the total enthalpy. Artifically-frozen vibrational energy was observed to have a much more influential role in increasing the shock stand-off distance than artifically-frozen chemical energy.[5] As mentioned above, the discrepancy was not observed for the same Mach number and stagnation enthalpy test condition in an expansion tube facility. This suggests that complex CO_2 vibrational relaxation processes may not be completely understood, in particular the inclusion of additional vibrational modes such as the symmetric streching and two bending modes. This work demonstrated the need for improved thermochemical modeling and additional experimental studies in different facilities for CO_2 flows.

At the cost of reduced test time and potential loss in core flow, expansion tubes are capable of producing high-enthalpy conditions while the degree of freestream non-equilibrium effects is significantly reduced in comparison to reflected shock tunnels. In the present work, the Hypervelocity Expansion Tube (HET) facility is used to investigate the effect of thermochemistry on shock-stand off distances in hypervelocity CO_2 flow to provide additional data to address the issues raised at the CUBRC facilities. We first identify and verify a suitable test condition with first-order matching of the high-enthalpy CUBRC test case. Next, spherical models of different diameter (7.9 to 63.5 mm) are examined as a canonical flow field for which shock stand-off distance data are obtained for equilibrium, non-equilibrium, and frozen conditions. These data are useful for validation of computational simulations and thermochemical models, as well as for additional verification of facility operation. In a Mach 5.7 CO_2 freestream, shock profiles over a MSL model geometry at three flight angles of attack (0, 11 and 16 degrees) are obtained. Surface heat flux measurements were made using coaxial thermocouples at 45 degrees from the stagnation point for cylinder models constructed of both tool and stainless steel. Heat flux measurements are then made at selected locations along the MSL model forebody at angles of attack.

A. Thermochemistry of Carbon Dioxide in Ground Test Facilities

The significance of thermochemical effects in high temperature carbon dioxide flows has been reported in a broad range of applications from high-energy lasers to Martian exploration. Relative to dissociation energy, vibrational energy is an order of magnitude more important in carbon dioxide than in nitrogen, see for example Rock et al.[6] For Martian planetary entry, predicting the aerothermodynamic loading on a vehicle is critical and the role of thermochemical effects has been pointed out in numerous studies.[7–9] For example, the increase in transition Reynolds number with increasing stagnation enthalpy was found to be significantly more pronounced in carbon dioxide than in nitrogen.[10,11]

In addition to its importance in flight, carbon dioxide thermochemistry can also be significant in flow acceleration to hypersonic velocities in ground testing facilities. As discussed above, the sensitivity of the CO_2 freestream to changes in internal energy was evaluated using simulations in two types of hypersonic facilities at CUBRC: a reflected shock tunnel and an expansion tube.[5] In the LENS I reflected shock tunnel, the shock stand-off distance was found to be significantly greater than the value predicted by numerical simulations and measured in the LENS X expansion tube.[5]

Shock tunnels have been used to create hypersonic CO_2 flows over blunt bodies by several research groups. An experimental and a perfect-gas numerical study of shock-stand off distances in Mach 5.75 flows over a blunted cone with nose radius 17.5 mm was carried out in the HST2 shock tunnel facilty by Jagadeesh et al.[12,13] Good agreement was observed between computational and experimental results in air and in carbon dioxide, however this study was carried out at a low free stream temperature, on the order of 150 K.

In high temperature CO_2, shock profiles over blunt bodies have been measured in the T3 and T5 reflected shock tunnels. Comparisons with numerical simulations of shock layer density over a sphere with experiments in T3 were made by Rock et al.[6] Good agreement was obtained between experiments and simulations, see also Candler.[14] Heat transfer to a scaled MSL model at angles of attack was measured in the T5 reflected shock tunnel.[15] Simulations were in good agreement with experiments when a supercatalytic wall was assumed in the laminar case, and whan a noncatalytic wall was assumed in the turbulent case. The reason for the discrepancy was unknown.

In the reflected shock tunnel HEG, CO_2 flow over a blunt cone was studied using simulations and experiments by Netterfield et al.[16] Simulations predicted thermal equilibrium and chemical non-equilibrium in the forebody flowfield. While the heat transfer distribution along the model forebody was similar in experiments and computations, the absolute value of the heat transfer was 70 % lower in the experiments. Computations agreed with the Fay and Riddell correlation.[17] The boundary layer was thought to be in equilibrium, so this difference could not be attributed to catalysis. Experimental images of the shock profile were not reported.

Bow shock stand-off distances were measured over a 140 degree blunt angle cone (an early version of the MSL model) for a 14.3 MJ/kg pure CO_2 run condition using a reflected-shock in the NASA Ames 42-inch shock tunnel.[18] Of the three different gas mixtures investigated for the same blunt body, the maximum discrepancy between computation and experiment for the shock stand-off distance was observed for the pure CO_2 condition. Despite the similarity between NASA Ames high-enthalpy reflected shock tunnel test conditions and those at the LENS facility, the differences between numerical and experimental results were much less pronounced in the AMES facility than observed at CUBRC.

To the author's knowledge, the only shock profile data for high-enthalpy CO_2 flow created in an expansion tube are that of Holden et al.[1] In expansion tube facilities, chemical nonequilbrium can occur during the unsteady expansion, however, in contrast to reflected shock tunnels, freezing is not usually reported. Two studies have examined the acceleration of CO_2 to hypervelocity conditions in an expansion tube. The operation of the X1 expansion tube with CO_2 was characterized by pitot pressure measurements and simulations by Wegener et al.[19] One-dimensional simulations with a simple chemical model showed that for stagnation enthalpies of 88 and 141 MJ/kg, equilibrium chemistry was a good assumption during flow acceleration through the unsteady expansion fan. At conditions with lower enthalpies, neither frozen nor equilibrium models could match experiments. Nonequilibrium calculations were not performed. Two carbon dioxide test conditions in the JX-1 expansion tube were examined through Navier-Stokes simulations with thermochemical modeling by Mizuno et al.[20] Thermochemical nonequilibrium was only observed in the accelerator gas (also carbon dioxide in this case) in the thin region where the transmitted shock reached the end of the accelerator tube. The present work aims to contribute data to address outstanding issues in thermochemical modeling of high temperature CO_2 and to help explain facility-specific questions arising in recent experiments.

II. Experimental Setup

The HET is a 9.14 m long facility consisting of three sections (driver, driven, and accelerator) all with 150 mm inner bore diameter, initially separated by primary and secondary diaphragms, Figure 1. The initial gas pressure and composition can be varied to achieve nominal Mach number operating conditions between 3.0 to 7.5 and stagnation enthalpies of 4.5 to 8.0 MJ/kg. A more detailed description of the facility can be found in Dufrene et al.[21] Selected run conditions are verified through a series of wavespeed (via shock arrival) and both static and pitot pressure measurements obtained using a combination of dynamic pressure transducers (series transducers PCB 113A/B26) at different locations throughout the facility.

Shock stand-off distances are measured using a schlieren system consisting of a Xenon nanopulser (10 ns duration) white light source and pco.1660 (Cooke Coorporation) CCD camera. The system is triggered via the transmitted shock arrival at a 1MHz response pitot pressure transducer (PCB 113A26) sting-mounted in the test section 63.5 mm below the model centerline.

The spheres and MSL are mounted within the test section such that their axial centerlines approximately correspond with the tube centerline. The 11 and 16 degree angle of attack positions were achieved by mounting the MSL model on triangular spacer blocks, whose hypotenuse was angled at the desired angle of attack from the vertical. The spheres and MSL were made from Al 2024 and A2 tool steel respectively. With a major diameter of 50.8 mm, the MSL model used in this study is approximately 1/100th the size of the actual vehicle. The scaled down dimensions of the MSL were designed according to those specified in Hollis et al.[22] As with the actual vehicle, the model has a 70 degree sphere cone forebody, however the current model only has single conic (40 degree) aftbody whilst the actual vehicle is biconic.

The thermocouples used in these experiments are based on the design of Sanderson.[23] They are coaxial, 2.4 mm in diameter, type E (Constantan-Chromel), and mount flush with the surface of a model. The two coaxial elements are designed such that an extremely thin junction (on the order of 1 μm) is formed at the surface. This type of thermocouple gauge is used extensively in the T5

reflected shock tunnel,[23–25] where the high enthalpy test conditions result in adequate signal levels and the robust design of the gauges make them highly resistant to damage caused by particulates in the test gas as well as the large heat fluxes.[23] The output signal is processed by a differential amplifier circuit mounted exterior to the test section. This also serves to eliminate the effects of any extraneous electromotive forces generated by the thermocouple. The circuit gain is 1000 to maximize signal amplitude. Individual calibration of thermocouples is not necessary, since the temperature response of all common thermocouple types is well known. The NIST thermocouple reference tables were used to convert from voltage to temperature.[26] For more information regarding the development, testing and performance verification of the thermocouples please see Flaherty and Austin.[27]

The experimental set up for the spectroscopic experiments is described in more detail in Sharma et al.[28] Briefly, spectra were collected using a SPEX 270M spectrometer and visualized with a Princeton Instruments PI-MAX MG:512SB intensified CCD camera system. Exposure was set to 100 μs. At the focal plane of the spectrometer, the dispersion is approximately 0.29 nm/pixel, corresponding to a wavelength range of approximately 148 nm.

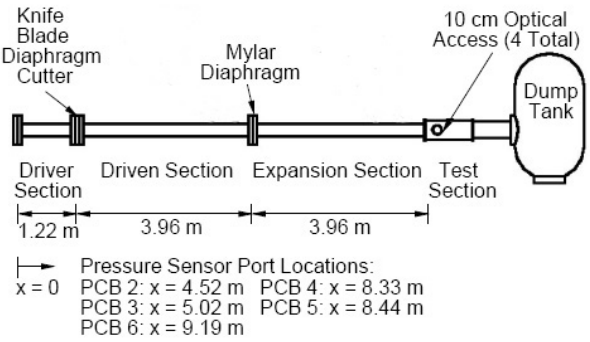

Figure 1: Schematics of the hypervelocity expansion tube (HET) facility.

III. Results

A. Criteria for Selection of Experimental Test Conditions

Carbon dioxide test gas conditions are selected with two goals in mind: i) to match relevant experimental parameters in CUBRC facilities as closely as possible and ii) to span frozen, nonequilibrium, and equilibrium test conditions as a function of model dimensions.

Since in general all test parameters cannot be matched from facility to facility, identification of the dominant flow properties for a particular measurement is important in comparative ground testing as well as in flight simulation. Simulations of blunt bodies in nitrogen flows by Macrossan showed that free stream dissociation had little effect on the bow shock at different angles of attack,[29] indicating that in nitrogen, the degree of dissociation in shock tunnel versus flight tests was less important to match than the Mach number. One aspect of the present study is to evaluate what parameters should be matched for adequate comparative measurements of shock profile and heat transfer for CO_2 flows in different expansion tube facilities.

The discrepancy between the CUBRC LENS X and LENS I results was observed for test conditions with 5.63 MJ/kg stagnation enthalpy in CO_2.[5] For the same stagnation enthalpy, we select the test gas velocity as the first-order matching parameter due to the large kinetic energy contribution to the total enthalpy. Matching the CUBRC condition in the HET requires a test gas velocity of 3036 m/s. Higher order matching could be achieved by using the frozen Mach number as a selection parameter, however the LENS X run condition frozen Mach number is 11.81, which is outside the operating regime of the HET.

As an expansion tube can cover a range of operating conditions, a parametric study based on steady, one-dimensional gas dynamic calculations is completed to select candidate test conditions. Additional criteria are then considered to achieve a well-characterized and uniform freestream. The expanded driver to driven gas sound speed ratio should be maintained below certain threshold values to reduce freestream disturbances.[21,30] The test time begins with the arrival of the driven to accelerator (secondary) gas interface and broadening of this interface should be minimized. Significant distortion of the contact surface and test time reduction was reported when carbon dioxide was used in both driven and accelerator sections in the JX-1 facilty.[20] Modeling the secondary interface as a contact surface undergoing horizontal acceleration f, we can treat the interface as susceptible to Rayleigh-Taylor instability with eigenvalue

$$s = \sqrt{\tilde{i} f \frac{(\rho_7 - \rho_6)}{(\rho_6 + \rho_7)}} \tag{1}$$

where state 7 denotes the test gas and state 6 denotes the accelerator gas. With no viscous effects f would be zero, however Mirel's effect[31] results in a positive contact surface acceleration. HET operating conditions always result in a positive density ratio (Atwood number) and thus the contact surface is temporally unstable. Increasing the Atwood number amplifies the instability and preliminary pitot pressure data for several run conditions show a corresponding broadening of the interface, corroborating this hypothesis. To reduce the Atwood number, air is selected as the accelerator gas.

For non-equilibrium flows, Lick applied inverse methods for the flow over a sphere[32] and his work was extended by Hall et al.[33] Using the ideal dissociating gas model, Hornung investigated non-equilibrium flow over spheres and cylinders.[34] Extending Hornung's original work, Wen and Hornung carried out a joint theoretical and experimental study of non-equilibrium dissociating flow over spheres and developed a model for the stand-off distance in terms of a reaction rate parameter.[35] Their model approximated the density profile as linear. A theoretical model for the non-equilibrium shock stand-off distance was also introduced by Belouggadia et al,[36] following an analytical solution proposed by Olivier.[37] The Olivier solution was confined to frozen and equilibrium flows, while the numerical model of Belouggadia et al. implemented calculated density profiles. At the post-shock to equilibrium density ratios in the present experiments, we find there is very little difference between density profiles calculated by the Wen and Hornung and Belouggadia et al. methods. As a result, the theory of Wen and Hornung will be used in this study.

The shock stand-off distance is known to be inversely proportional to the average density on the stagnation streamline.[34,35] The non-dimensional stand-off distance variation with the reaction rate parameter $\widetilde{\Omega}$, defined as the ratio of the energy absorption rate by chemistry to the free-stream kinetic energy input rate,[35] is shown in Figure 2 for four candidate test conditions with the same velocity and slightly different stagnation enthalpies. In the legend, the test conditions are described by the test gas Mach number, the initial driven and accelerator pressures and the accelerator gas

respectively. The theory indicates that, for a given sphere diameter, the shock stand-off distance is most sensitive to the test gas Mach number, as expected from the dependence on stagnation streamline density. Curves are very similar for all four candidate test conditions. Of particular importance to this study, results show decreasing Mach number increases the stand-off distance.

Based on the above considerations, a helium driver and air accelerator section test condition

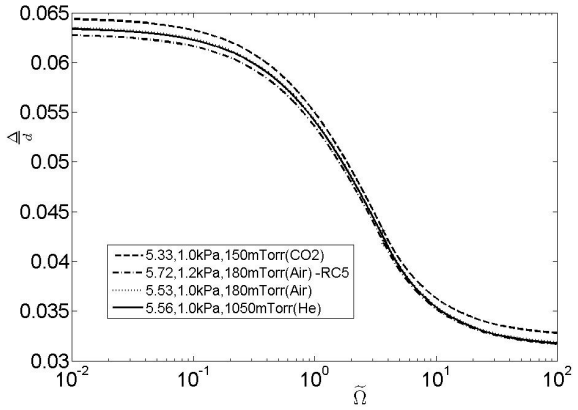

Figure 2: Comparison of non-dimensional shock standoff distances versus reaction rate parameter, based on the theory of Wen and Hornung,[35] for different proposed test conditions.

was selected and denoted as RC5. The test gas properties are computed with inviscid, unsteady one-dimensional gas dynamic calculations and are presented in Table 1 together with corresponding experimental measurements. u_s is the initial shock speed in the driven section and u_t is the transmitted shock velocity in the accelerator gas. Transmitted shock velocity is typically accurate to within ± 43 m/s in this facility, and it is expected that similar error bars will exist for test gas velocity measurements.[28] All the experimental values are averaged values across a number of realizations for repeatability. The pitot pressure measurements were obtained 6.35 mm below the tube centerline. Static pressure values were obtained at two stations, 30.48 cm and 55.88 cm, upstream from the tube exit.

There is a discrepancy between the experimental and theoretical pitot pressure value. The

	M_7	$h_{o,7}$ (MJ/kg)	Test Time (μs)	$P_{7,pitot}$ (kPa)	P_7 (kPa)	u_t (m/s)	u_7 (m/s)	u_s (m/s)
Experiment	–	–	150	82.09	2.71	3644	–	1832
Theoretical	5.7	5.67	274	128.26	3.2	3710	3058.8	1853

Table 1: Selected test condition parameters. Theoretical calculations assuming one-dimensional, perfect gas dynamics and compared with experimental measurements.

theoretical test gas pitot pressure is determined from the Rayleigh pitot equation. Perfect gas calculations show the pitot pressure is most sensitive to the static pressure across the secondary contact surface (states 6 and 7). To first-order, this dependence can be approximated as linear.

Accordingly, the measured static pressure would correspond to a pitot pressure of 109 kPa. Due to the high temperatures at the pitot probe stagnation point, it is possible that the perfect gas assumption is no longer applicable and thermochemistry must be considered.

The transmitted shock speed was also measured in the test section using the shock time-of-arrival at staggered pitot probes. This approach has been used in the past to characterize a test condition and in that instance, it was found that the measurement agreed with computational results.[38] Experimental pitot surveys of the core flow at this test condition were carried out to determine that the maximum model diameter that can be chosen is about 65 mm.

B. Sphere shock profiles

We initially examine spherical models in benchmark tests for which results can be compared with existing experimental data and theoretical predictions. This flowfield provides the potential for additional verification of facility operation via numerical simulations and thermochemical calculations with a relatively simple geometry. Shock stand-off distances over a sphere have been previously investigated in non-equilibrium air and nitrogen flows.[34,39] As discussed in Section I, shock stand-off distances in carbon dioxide have been measured in the Caltech T5 reflected shock tunnel facility.[35] Despite the extensive contributions of these previous studies, outstanding issues in a carbon dioxide flowfield still remain, including the role of thermochemical energy storage and transfer and the possibility of facility-specific data. Therefore, the measurement of the shock stand-off distance for similar enthalpy conditions in another hypervelocity facility provide data to complement existing results.

Selected schlieren images for spheres of diameters from 25.4 to 63.5 mm are shown in Figure 3a-d.

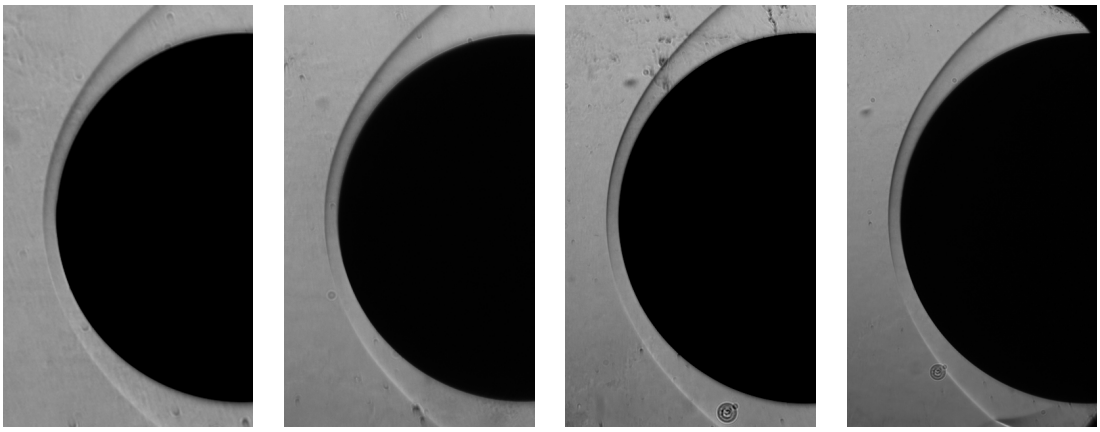

a) b) c) d)

Figure 3: Comparisons of experimental schlieren images and simulations of bow shock profiles over spheres of diameter a) 25.4 mm, b) 37.5 mm, c) 50.8 mm, and d) 63.5 mm. Note that the images have been scaled for visual purposes.

Wen and Hornung presented analytical expressions for the transition point between the non-equilibrium and equilibrium regions.[35] For the RC5 test condition, the variation of non-dimensional stand-off distance with the reaction rate parameter is shown in Figure 4. Transition is predicted when the non-dimensional shock stand-off distance is 0.042. The figure was generated

using the equilbrium density for the specified inflow conditions.[40] Varying the sphere diameter will adjust the density profile in a monatonic fashion.[35] As the sphere diameter is increased, for the same run condition, the flow along the stagnation streamline transitions from non-equilibrium conditions throughout to a profile with an equilibrium region close to the body.

From Figure 4, one can see that for a 50.8 mm sphere the equilibrium and frozen stand-off

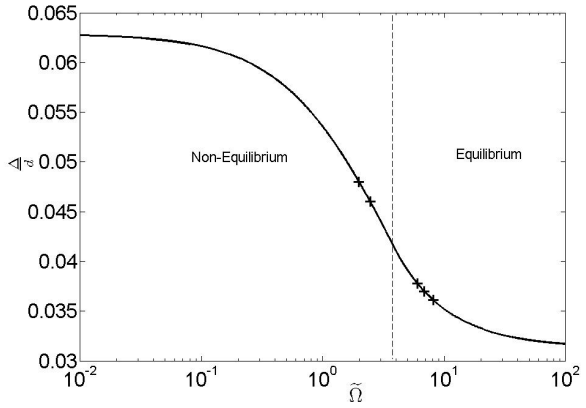

Figure 4: Non-dimensional shock stand-off distance versus the reaction rate parameter for RC5 based on the results of Wen and Hornung.[35] The predicted transition from non-equilibrium to equilibrium is shown as the dashed line. The black crosses denote the results from the current experiments.

distance limits are approximately 1.63 mm and 3.2 mm respectively. The results are summarized in Table 2. For each diameter, the corresponding reaction rate parameter is also listed. For example, for the 25.4 mm diameter sphere, the non-dimensional stand-off distance is 0.045, corresponding to a reaction rate parameter of 2.45. Physically, this means that the rate of absorption by chemistry is roughly 2.5 times greater than the kinetic energy input rate. This value is just above the transition point value of 0.042 and flow is predicted to remain in non-equilibrium. These results are also plotted on Figure 4. Based upon the transition location, it can be seen that increasing the sphere diameter is predicted to result in the shock layer transitioning from a non-equilibrium to an equilibrium profile.

Sphere diameter (mm)	Measured stand-off distance (mm)	$\widetilde{\Omega}$
63.5	2.29	8.09
50.8	1.89	6.82
38.1	1.44	5.97
25.4	1.13	2.45
7.9	0.38	1.98

Table 2: Measured shock stand-off distances for different sphere diameters.

C. Shock Profiles at Angle of Attack

Experimental images of the bow shock profile over the MSL geometry at three angles of attack are shown in Figure 5. Images show increasing shock stand-off distance with increasing angle of attack. In the non-zero angle of attack images, in particular for the 16 degree case, the shock appears to be spherically shaped on the windward side and more conically shaped over the leeward side. Similar results were also observed by Stewart and Chen.[18] For the 16 degree case, Figure 5 c), the maximum bow shock gradient with respect to the horizontal (freestream) has shifted towards the windward side. The vertical shift of this location is 8.5 mm. We compare the measured shock profile at zero angle of attack with the experimental results from previous studies, Figure 5. Good agreement is observed with profiles measured in the LENS X expansion tube.[1]

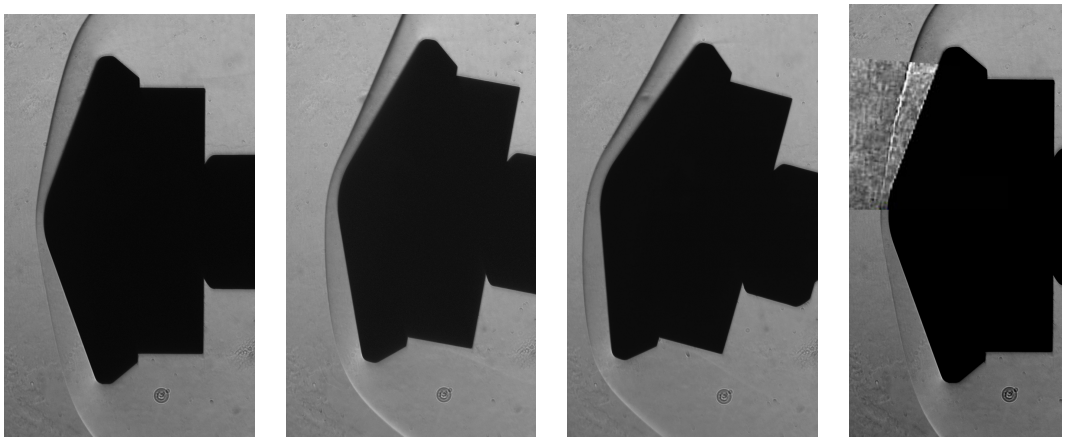

a) b) c) d)

Figure 5: Experimental schlieren images, of bow shock profiles over the MSL geometry at angles of atack of a) 0 , b) 11, c) 16 degrees and d) Comparison of 0 degree bow shock profile with previous CUBRC LENS X data.[41]

D. Laminar Heat Flux and Catalytic Heating

Heat transfer measurements have been extensively used in aerothermodynamic studies of transition,[15,22] of surface catalysis[15,42] or as a means to capture spatial profile behavior[18] in CO_2. Extensive investigations into the influence of wall catalysis boundary conditions upon surface heating in high-enthalpy carbon dioxide flow fields have been completed in the LENS facilities.[22,42] MacLean and Holden compared heat transfer results with different catalytic boundary conditions. Discrepancies between the experimental surface heat transfer results and computation in the reflected shock tunnel facilities for three different high-enthalpy CO_2 run conditions (5.63, 5.99 and 8.65 MJ/kg)[42] were observed. At the low-enthalpy condition (1.89 MJ/kg), the overall agreement was very good. MacLean and Holden conclude that freestream uncertainty, and hence vibrational relaxation processes within the nozzle, is a contributing factor to, although not a full explaination of, these differences. Results from the CUBRC studies found that the experimental heating rates fell in-between non-catalytic and super-catalytic boundary conditions, which suggested that finite-

rate catalysis existed at all points on the surface.[42]

We first measure the stagnation point heat flux measurements on a 25.4 mm diameter stainless steel sphere. Based upon three repeat experiments, the average heat flux across the test time is found to be 6.73±0.55 MW/m^2. The semi-empirical prediction of Sutton and Graves[43] is 6.85 MW/m^2, which agrees well with the experimental result. Since the MSL model was constructed of tool steel, two cylindrical models, one of 316 stainless steel and one of A2 tool steel were next tested. Both cylinders were instrumented with a gauge mounted on the vertical axis of symmetry at a 45 degree angle. Figure 6 shows the comparison between two gauges in terms of the detected temperature rise. The temporal offset occurs only due to shot-to-shot variation in triggering. For heat transfer calculation, it is the gradient of the temperature history that is important and, as shown in Figure 6, the gradients appear to be very similar. At the 45 degree location, the average heat flux measured in repeat experiments was 2.55 MW/m^2 and 2.53 MW/m^2 on the tool and stainless steel models respectively. It is concluded that the heat flux measurements are not influenced by model material for these two steels.

The MSL model was instrumented with 11 thermocouples along the line of symmetry, with

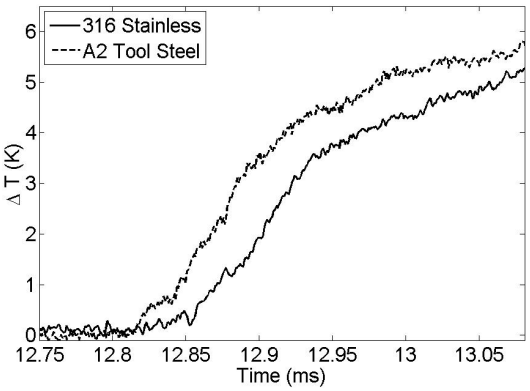

Figure 6: Change in temperature time history traces detected by two different thermocouples on A2 and 316 stainless steel cylinder models.

5 on each side of the nose location. Repeat experiments were conducted for each of the three angle of attack conditions. Heat transfer measurements at selected locations are shown in Figure 7, corresponding to the nose tip and ± 4.3, 8.6 and 17 mm offset from the nose tip. To be consistent with previous studies, the windward side is defined to be negative for a positive angle of attack. For a zero degree angle of attack, the average measured heat flux is 6.35±0.5 MW/m^2. For the same condition, stagnation point measurements for a 25.4 mm sphere (same radius as the MSL nose radius of curvature) were 6.73 MW/m^2. The results from Figure 7 capture the general trends observed in previous MSL studies at CUBRC.[22] The nose heat transfer decreases with increasing angle of attack, which is indicative of the stagnation point shifting to the windward side as observed in Figures 5 a)-c). At 16 degrees, the average measured heat flux was 4.95MW/m^2, which is approximately a 22 % reduction compared to the 0 degree configuration. On the windward side, the heat fluxes appear to be invariant with angle of attack for the angles considered, a feature also previously observed in the LENS I facility.[22] Additionally, the asymmetric nature of the curve has been captured at the 11 and 16 degree cases, whereby the leeward side measurements (at the

same radial location magnitude) are lower than those on the windward side. For the current MSL model, no transition is expected or observed given the Reynolds Number of flow and the scale of the model.

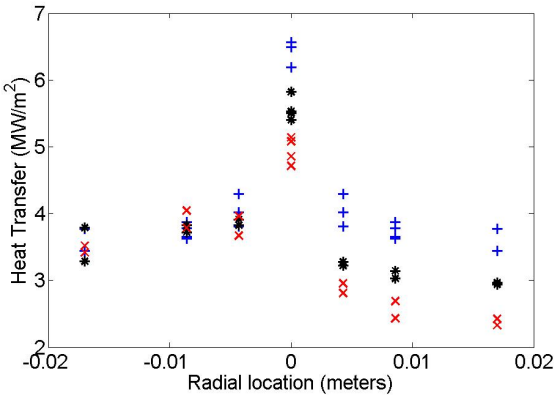

Figure 7: Heat flux measurements along the centerline of the MSL geometry at three angles of attack: 0(+), 11($\star$), and 16 degrees($\times$).

E. Emission Spectroscopy Measurements

Previous work has developed and demonstrated the application of emission spectroscopy for species identification and temperature measurements in the HET.[28] Vibrational temperature measurements based on OH emission spectra were made in the relaxation region behind the normal shock created via a Mach reflection.[44] The experimental method was extended to obtain NO-based temperature measurements for the same flow field.[28]

Emission spectroscopy using atomic, rather than molecular, species presents several advantages. The absence of rotational and vibrational internal energy modes significantly reduces the complexity of the spectral signature. Flow field temperature can be calculated based upon line intensity, Equation 2.

$$I = G g_{ul} A_{ul} \upsilon_{ul} e^{\frac{-1.4387\varepsilon}{T}} \tag{2}$$

where g is the degeneracy, ε is the energy change of the transition, A_{ul} is the Einstein spontaneous emission co-efficient, υ_{ul} is the frequency, T is the temperature and G are optical constants relating to the setup. For an equilibrium flow field, using the ratio of two line intensities (measured experimentally), this equation can be used to extract temperature based upon the transition energies. Atomic emission lines, particulary for metallic species, are generally very well characterized.

It is proposed to measure flow field temperatures based upon the emission of trace amounts of metallic species, which are present after the dissociation of organometallic compounds (OMC) due to very high temperatures behind a hypersonic shock front. Emission spectroscopy only requires very small concentrations (on the order of parts-per-million or even less) since it probes the upper states. Measurement within the equilibrium portion of the shock layer ensures that the measured species temperature corresponds to the CO_2 flow field temperature. The following criteria are

identified as key requirements for any potential metal organic compound.

1. Sufficiently safe by typical lab standards, specifically not a toxic, flammable or corrosive material. On the Hazard Materials Identification System, the health, flammability and reactivity ratings should all below 2.
2. Sufficiently volatile with a vapor pressure high enough that the compound is a liquid at room temperature and vaporizes at pressures above the test condition initial driven pressure.
3. The two selected lines for temperature measurement have intensities that differ by no more than 90 %
4. Selected lines exist in a wavelength range without considerable background emission from other species
5. Fine-scale spectral resolution such that the two selected lines will be separated, at maximum, by only 30 nm (optional)

The intensity ratio consideration exists to allow single-shot comparison. In other situations, highly disparate intensity lines can be used for temperature calculation, however, this requires two experiments with differing exposure times - an option that is not available for the HET. The last requirement is quite restrictive, and therefore optional only. Temperature measurements can still be conducted using coarse-scale measurements, however, fine-scale measurements will permit greater accuracy and prevent "amalgamation" with neighbouring lines.

Based upon the above considerations, it was decided to use the organo-metallic compound, tetraethoxysilane, in order to access ultraviolet atomic silicon emission. A sample spectra was collected 1 mm directly upstream from the stagnation point of a 50.8 mm sphere, Figure 8. Radiation from atomic silicon, the OH A-X and the CH C-X band is identified. The silicon emission at 252 nm consists of multiple transitions which have merged into a single, broad peak due to the coarse spectral resolution. The second silicon emission at 288 nm is clear. Background signals are present around these two lines, which are currently significant enough to influence a temperature calculation. Different organo-metallic compounds, and their associated metallic constituents, are being investigated to provide more pronounced lines whose emission is not amongst other species radiation. The results demonstrate that organo-metallic emission spectroscopy is a viable technique as dissociation of the vaporized compound and atomic emission can be observed.

IV. Conclusions and Future Work

Experimental measurements of shock profiles and heat flux over canonical blunt bodies and a Mars Science Lander model have been conducted in a hypervelocity carbon dioxide flow. This study was motivated by previous experiments at the CUBRC family of hypervelocity facilities which found that substantially different shock stand-off distances were measured in different impulse facilities. One contributing factor is that the free stream carbon dioxide thermochemistry is dependent on the means via which the flow is accelerated to high velocities. To address this question and provide complementary results to those from CUBRC, present experiments are carried out in the Hypervelocity Expansion Tube.

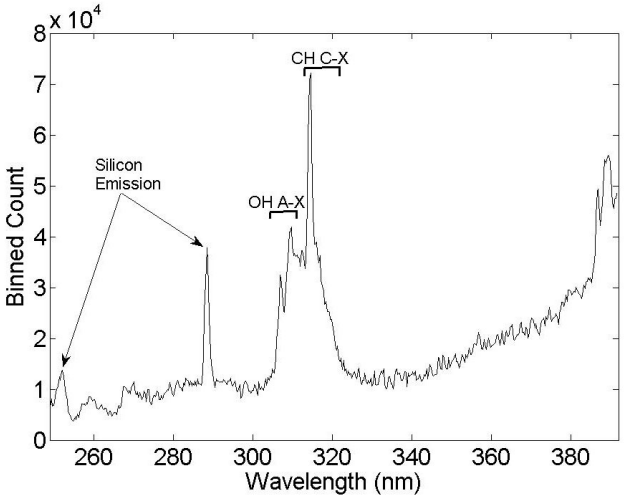

Figure 8: Spectra collected at 1 mm upstream of 50.8 mm sphere stagnation point. Atomic Silicon, OH A-X and CH C-X band emissions are identified.

A test condition, labeled RC5, was selected to match the CUBRC MSL test conditions by matching the stagnation enthalpy (5.63 MJ/kg) and the velocity (2900 m/s). Spheres with varying diameters were chosen as benchmark models for which shock stand-off distances could be compared with existing data and theory. The theory of Wen and Hornung [35] predicts, that for RC5, the range of diameters chosen spans frozen, non-equilibrium and equilibrium stagnation streamlines flows which was important information for on-going spectroscopic studies. Sphere stagnation point heat transfer measurements were in good agreement with existing fits which assumed a noncatalytic boundry condition.

A scaled MSL model was next tested in this flow field. Shock profiles and heat transfer measurements were obtained at three different angle of attacks: 0, 11, and 16 degrees. Excellent agreement was obtained in the shock profiles measured in both the CUBRC expansion tube and HET facility, implying the stagnation enthalpy and velocity are reasonable first-order matching parameters for these measurements in different expansion tube facilities. The results confirm facility-independence for the same type of flow acceleration. The heat transfer data followed the general trends observed in previous experiments. Peak-heating shifted to the windward side with non-zero angle of attack. Windward side heat transfer values appear quite insensitive to angle of attack, while the leeward side values decrease appreciably with increasing angle of attack.

Results from a proposed novel emission spectroscopy technique using atomic emission from an organo-metallic compound to measure flow field vibrational temperatures are presented. Results so far are reasonably promising as atomic emission has been detected, indicating that, provided background contamination can be eliminated, organo-metallic compound emission spectroscopy shows potential for non-intrusive temperature measurement behind the shock front in hypervelocity carbon dioxide flow.

References

[1]Holden, M. S., Wadhams, T. P., MacLean, M., Mundy, E., and Parker, R. A., "Experimental studies in LENS I and X to evaluate real gas effects on hypervelocity vehicle performance," *45th AIAA Aerospace Sciences Meeting and Exhibit, Reno, Nevada*, 2007.

[2]Holden, M. S. and Candler, G. V., "Experimental Studies in the LENS Shock Tunnel and Expansion Tunnel to Rxamine Real-Gas Effects in Hypervelocity Flows," AIAA Paper 2004-0916, Jan. 2004.

[3]I.Nompelis, Candler, G. V., and Holden, M. S., "Effect of Vibrational Nonequilibrium on Hypersonic Double-Cone Experiments," *AIAA Journal*, Vol. 41, No. 11, 2003, pp. 2162–2169.

[4]C.Park, "Thermochemical Relaxation in Shock Tunnels," *Journal of Thermophysics and Heat Transfer*, Vol. 4, No. 4, 2006, pp. 690–698.

[5]MacLean, M. and Holden, M. S., "Numerical Assesment of Data in Catalytic and Transitional Flows for Martian Entry," *9th AIAA/ASME Joint Thermophysics and Heat Transfer Conference*, 2006.

[6]Rock, S. G., Candler, G. V., and Hornung, H. G., "Analysis of Thermochemical Nonequilibrium Models for Carbon Dioxide Flows," *AIAA Journal*, Vol. 31, No. 12, 2003, pp. 2255–2262.

[7]Chen, Y. K., Henline, W. D., Stewart, D. A., and Candler, G. V., "Navier-Stokes solutions with surface catalysis for Martian Atmospheric entry," *Journal of Spacecraft and Rockets*, Vol. 30, No. 1, 1993, pp. 32–42.

[8]Gnoffo, P. A., Braun, R. D., Weilmuenster, J. K., Mitcheltree, R. A., Engelund, W. C., and Powell, R. W., "Prediction and Validation of Mars Pathfinder Hypersonic Aerodynamic Database," *Journal of Spacecraft and Rockets*, Vol. 36, No. 3, 1999, pp. 367–373.

[9]Sarma, G. S. R., "Physio-chemical modelling in hypersonic flow simulation," *Progress in Aerospace Sciences*, Vol. 36, No. 3-4, 2000, pp. 281–349.

[10]Germain, P. D. and Hornung, H. G., "Transition on a slender cone in hypervelocity flow," *Experiments in Fluids*, Vol. 22, No. 3, 1997, pp. 183–190.

[11]Adam, P. H. and Hornung, H. G., "Enthalpy effects on hypervelocity boundary-layer transition: Ground and flight test data," *Journal of Spacecraft and Rockets*, Vol. 34, No. 5, 1997, pp. 614–619.

[12]Jagadeesh, G., Sun, M., Nagasheetty, K., and Reddy, K. P. J., "Experimental investigations of test gas effects on the hypersonic flow field around large angle blunt cone in shock tunnel," *39th AIAA Aerospace Sciences Meeting, 8-11 January 2001, Reno NV, AIAA paper 2001-0305*, 2001.

[13]Jagadeesh, G., Nagasheetty, K., Reddy, K. P. J., Sun, M. Y., and Takayama, K., "Studies on the effects of test gas on the flow field around large angle blunt cone flying at hypersonic Mach number," *Transactions of the Japan Society for Aeronautical and Space Sciences*, Vol. 45, No. 149, 2002, pp. 189–194.

[14]Candler, G. V., Mavriplis, D., and Trevino, L., "Current Status and Future Prospects for the Numerical Simulation of Hypersonic Flows," *47th AIAA Aerospace Sciences Meeting and Exhibit*, 2009.

[15]Wright, M. J., Olejniczak, J., Brown, J. L., Hornung, H. G., and Edquist, K. T., "Modeling of shock tunnel aeroheating data on the Mars Science Laboratory Aeroshell," *J. Thermophysics and Heat Transfer*, Vol. 20, No. 4, 2006, pp. 641–651.

[16]Netterfield, M. P., Mazoue, F., Marraffa, L., Kastell, D., and Eitelberg, G., "Experiments and computations on a blunt body in high enthalpy CO_2," *31st AIAA Thermophysics and Heat Transfer Conference, 17-20 June 1996, New Orleans LA, AIAA paper 1996-1804*, 1996.

[17]Fay, J. A. and Riddell, F. R., "Theory of stagnation point heat transfer in dissociated air," .

[18]Stewart, D. A. and Chen, Y. K., "Hypersonic convective heat transfer over 140-deg blunt cones in different gases," *Journal of Spacecraft and Rockets*, Vol. 31, No. 5, 1994, pp. 735–743.

[19]Wegener, M., Sutcliffe, M., Morgan, R., McIntyre, T., and Rubinsztein-Dunlop, H., "Diagnostics of a Range of Highly Superorbital Carbon Dioxide Flows," *39th AIAA Aerospace Sciences Meeting and Exhibit*, 2001.

[20]Mizuno, H., Sawada, K., and Sasoh, A., "Numerical analysis of carbon dioxide flowfield in expansion-tube," *8th AIAA/ASM Joint Thermophysics and Heat Transfer Conference, 24-26 June 2002, St. Louis, Missouri, AIAA paper 2002-3221*, 2002.

[21]Dufrene, A., Sharma, M., and Austin, J. M., "Design and characterization of a hypervelocity expansion tube facility," *Journal of Propulsion and Power*, Vol. 23, No. 6, 2007, pp. 1185–1193.

[22]Hollis, B. R., Leichy, D. S., Wright, M. J., Holden, M. S., Wadhams, T. P., MacLean, M., and Dyakonov,

A., "Transition Onset and Turbulent Heating Measurements for the Mars Science Laboratory Entry Vehicle," *43rd AIAA Aerospace Sciences Meeting and Exhibit*, 2005.

[23]Sanderson, S. R., *Shock wave interaction in hypervelocity flow*, Ph.D. thesis, California Institute of Technology, Pasadena, California, 1995.

[24]Davis, J.-P., *High-Enthalpy Shock/Boundary-Layer Interaction on a Double Wedge*, Ph.D. thesis, California Institute of Technology, Pasadena, California, 1999.

[25]Rasheed, A., *Passive Hypervelocity Boundary Layer Control Using an Ultrasonically Absorptive Surface*, Ph.D. thesis, California Institute of Technology, Pasadena, California, 2001.

[26]Croarkin, M. C., Guthrie, W. F., Burns, G. E., Kaeser, M., and Strouse, G. F., "Temperature-Electromotive Force Referance Function and Tables for the Letter-Designated Thermocouple Types Based on the ITS-90." Monograph 175, National Institute of Standard Technologies, 1993.

[27]Flaherty, W. and Austin, J. M., "Comparative Surface Heat Transfer Measurements in Hypervelocity Flow," *48th AIAA Aerospace Sciences Meeting and Exhibit*, 2010.

[28]Sharma, M., Austin, J. M., Glumac, N. G., and Massa, L., "NO and OH Spectroscopic Vibrational Temperature Measurements in a Post-Shock Relaxation Region," *submitted to the AIAA Journal*.

[29]Macrossan, M. N., "Hypervelocity flow of dissociating nitrogen downstream of a blunt nose," *Journal of Fluid Mechanics*, Vol. 217, 1990, pp. 167–202.

[30]Paull, A. and Stalker, R. J., "Test flow disturbances in an expansion tube," *Journal of Fluid Mechanics*, Vol. 245, 1992, pp. 493–521.

[31]Mirels, H., "Shock Tube Test Time Limitation Due to Turbulent-Wall Boundary Layer," *AIAA Journal*, Vol. 2, No. 10, 1963, pp. 84–93.

[32]Lick, W., "Inviscid flow of a reacting mixture of gases around a blunt body," *Journal of Fluid Mechanics*, Vol. 9, No. 1, 1960, pp. 128–144.

[33]Hall, J. G., Eschendoeder, A. Q., and Marrone, P. V., "Blunt-nose inviscid ariflows with coupled non-equilibrium processes," *Journal of Aeronautical Space Sciences*, Vol. 29, No. 9, 1962, pp. 1038–1051.

[34]Hornung, H. G., "Non-equilibrium dissociating nitrogen flows over spheres and circular cylinders," *Journal of Fluid Mechanics*, Vol. 53, 1972, pp. 149–176.

[35]Wen, C. Y. and Hornung, H. G., "Non-equilibrium dissociating flow over spheres," *Journal of Fluid Mechanics*, Vol. 299, 1995, pp. 389–405.

[36]Belouaggadia, N., Olivier, H., and Brun, R., "Numerical and theoretical study of the shock stand-off distance in non-equilibrium flows," *Journal of Fluid Mechanics*, Vol. 607, 2008, pp. 167–197.

[37]Olivier, H., "A theoretical model for the shock stand-off distance in frozen and equilibrium flow," *Journal of Fluid Mechanics*, Vol. 413, 2000, pp. 345–353.

[38]McGilvray, M., Austin, J. M., Sharma, M., Jacobs, P. A., and Morgan, R. G., "Diagnostic modelling of an expansion tube operating condition for a hypersonic shear layer experiment," *Proceedings of the 16th Australasian Fluid Mechanics Conference*, 2007.

[39]Wegener, P. P. and Buzyna, G., "Experiments on shock stand-off distance in non-equilibrium flow," *Journal of Fluid Mechanics*, Vol. 37, pt. 2, No. 2, 1969, pp. 325–335.

[40]McBride, B. J. and Gordon, S., "Computer Program for Calculation of Complex Chemical Equilibrium Compositions and Applications, II. Users Manual and Program Description," NASA CR-1311, 1996.

[41]Holden, M. S., Wadhams, T. P., MacLean, M., and Mundy, E., "Experimental Studies in LENS I and X to Evaluate Real Gas Effects on Hypervelocity Vehicle Performance," *45th AIAA Aerospace Sciences Meeting and Exhibit*, 2007.

[42]Holden, M. S. and MacLean, M., "Catalytic Effects on Heat Transfer Measurements for Aerothermal Studies with CO_2," *44th AIAA Aerospace Sciences Meeting and Exhibit*, 2006.

[43]Sutton, K. and Graves, A. R., "A general stagnation-point convective-heating equation for arbitary gas mixtures," Tech. rep., NASA, 1971.

[44]M.Sharma, Austin, J. M., and Glumac, N. G., "Effect of Thermochemistry on Mach Reflection in Hypervelocity Flow," AIAA Paper 2008-5066, July 2008.